

<https://doi.org/10.1038/s41612-024-00882-0>

# Seasonal phase change of the North Atlantic Tripole Sea surface temperature predicted by air-sea coupling

Haipeng Yu<sup>1</sup>✉, Shanling Cheng<sup>1,2</sup>, Jianping Huang<sup>3</sup>, Zeyong Hu<sup>1</sup>, Haojie Wu<sup>1,2</sup> & Xin Wang<sup>4</sup>

The North Atlantic Tripole sea surface temperature anomaly (NAT SSTA) is critical for predicting climate in Eurasia. Predictions for summer climate anomalies currently assume the NAT SSTA phase persists from boreal winter through summer. When NAT phase switches, predictions become unreliable. However, the NAT phase sustained/reversal mechanism from boreal winter to spring remains unclear. This study demonstrates that the evolution of the NAT phase could be driven by the North Atlantic Oscillation (NAO). When NAO phase persists (switches) during preceding boreal winter, the NAO-driven wind anomalies favor maintenance (transition) of NAT phase by causing sea surface heat flux anomalies. Meanwhile, NAT SSTA causes eddy-mean flow interaction by increasing atmospheric baroclinity, thereby generating positive feedback on the former NAO phase. The NAO phase change is leading 1–3 months for the NAT phase. These findings deepen our understanding of the interaction between NAO and NAT and provide implications for seasonal prediction in Eurasia.

The North Atlantic is located upstream of Eurasia, whose sea surface temperature anomaly (SSTA)<sup>1,2</sup> is often closely linked to climatic anomalies in Eurasia and thus provides valuable information for climate prediction in this region. On the interdecadal scale, North Atlantic SST exhibited prominent multidecadal fluctuations with alternating warm and cool phases<sup>1</sup>. On the interannual and seasonal scales, it is a tripole pattern. The positive phase of the North Atlantic Tripole sea surface temperature anomaly (NAT SSTA) presents a spatial distribution of “cold-warm-cold” from south to north, while the negative phase is opposite<sup>3</sup>. Several studies have demonstrated the pronounced impacts of the NAT SSTA on the weather and climate of Eurasia<sup>4–7</sup>. In boreal winter, NAT SSTA drives the atmosphere through surface heat flux, which not only impacts temperatures and precipitation in Eurasia but also has a profound effect on planet-scale atmospheric teleconnection<sup>4,6</sup>. In spring and summer, NAT SSTA influences the weather and climate of Eurasia mainly through three potential ways<sup>4–6</sup>. Currently, the most researched potential way is for NAT SSTA to stimulate a Rossby wave train propagating along the westerly jet, which propagates eastward and results in climate anomaly in Eurasia<sup>3,4,8</sup>. The second way is that the SSTA stimulates Kelvin waves to transport the signal from the tropical Atlantic to the Indian and impacts atmospheric circulation and SST in the Indian Ocean, resulting in temperature and precipitation anomalies in Eurasia<sup>9,10</sup>. The third way is that the North Atlantic SSTA influences the

Walker circulation and tropical East Pacific SST, leading to the Eurasia summer atmospheric circulation anomalies<sup>6,11</sup>.

The NAT SSTA is a key factor in influencing climatic anomalies in Eurasia. It is the persistence and slow variation of SST that the North Atlantic SSTA is of great indicative significance for predicting precipitation and temperature in Eurasia. While the NAT SSTA phase is always assumed to be maintained from boreal winter to summer currently when predicting summer climate anomalies in the preceding winter<sup>3,4</sup>, our analysis finds (Fig. S1) that the phase of NAT SSTA is prone to switch in boreal winter (reach 53%), with the highest frequency of switch occurring in December. The two opposite phases of the NAT SSTA are accompanied by distinct storm tracks over the North Atlantic and different weather and climate anomaly patterns in Eurasia<sup>3,4,12–14</sup>. The prediction would be invalid in the NAT SSTA phase switching years under the assumption of NAT SSTA phase persisting. Thus, it is important to reveal the physical mechanism of the persistence/switch of the NAT SSTA phases.

The North Atlantic Oscillation (NAO) is the dominant mode of interannual variability in atmospheric circulation over the North Atlantic<sup>15</sup>. It reflects the sea level pressure (SLP) difference between the Subtropical (Azores) and the Subpolar. On the interannual and seasonal scale, the formation and maintenance of NAT SSTA are largely influenced by NAO<sup>16</sup>. Previous studies have shown that NAO anomalies primarily drive SSTA

<sup>1</sup>Key Laboratory of Cryospheric Science and Frozen Soil Engineering, Nagqu Plateau Climate and Environment Observation and Research Station of Tibet Autonomous Region, Northwest Institute of Eco-Environment and Resources, Chinese Academy of Sciences, Lanzhou, China. <sup>2</sup>University of Chinese Academy of Sciences, Beijing, China. <sup>3</sup>Key Laboratory for Semi-Arid Climate Change of the Ministry of Education, College of Atmospheric Sciences, Lanzhou University, Lanzhou, China. <sup>4</sup>College of Earth and Environmental Sciences, Lanzhou University, Lanzhou, China. ✉e-mail: [yuhp@lzb.ac.cn](mailto:yuhp@lzb.ac.cn)

changes through two pathways<sup>17–21</sup>. On the one hand, the NAO-related wind anomalies may lead to the formation and maintenance of NAT SSTA through surface heat fluxes over the North Atlantic<sup>17,19</sup>. On the other hand, in midlatitudes, NAO-related atmospheric circulation anomalies can induce SSTA by meridional current, and Ekman pumping<sup>18,20,22,23</sup>. In turn, the North Atlantic SSTA may feedback on the atmospheric circulation<sup>8,17,24,25</sup>. The NAT SSTA may drive anomalous storm tracks and modulate the eddy activity through anomalous meridional SST gradient and surface temperature gradients. The anomalous eddy activity then modifies the low-frequency mean flow through the convergence of the eddy momentum flux<sup>26</sup>. The synoptic-scale eddy activities may impact the atmosphere through two potential ways in midlatitudes: eddy vorticity (EV) flux forcing and eddy heat (EH) flux forcing<sup>8,18,27–29</sup>. The varying contributions of the above mechanisms may lead to different types of atmospheric circulation responses<sup>28,30</sup>, resulting in a more complex feedback of the SSTA on mid-latitudes atmospheric circulation.

Previous researches have indicated inconsistent results regarding feedback of NAT SSTA on the NAO<sup>26,31–35</sup>. Some investigations suggest that mid-latitude SSTAs tend to exert positive feedback on the atmosphere, lengthening the former atmospheric circulation anomalies<sup>24,32,36</sup>. On the other hand, certain observational studies indicate that the SSTA feedback may not maintain the previous atmospheric circulation forcing, but instead tends to leading a nearly reversed pattern<sup>26,33,37</sup>. While the North Atlantic air-sea coupling processes have been extensively studied in previous research<sup>8,14,18,26,30</sup>, the mechanisms of NAT SSTA phases maintenance or transformation from boreal winter to spring remain unclear, and how the NAT SSTA feedback on NAO remains an open question. Therefore, we utilized various diagnostic analysis methods to reveal the

physical mechanism of NAT SSTA phase persistence or transition from boreal winter to spring and clarify the relationship between NAO and NAT SSTA. Our findings offer insights into the factors influencing NAT SSTA phase changes, providing a scientific foundation for enhancing seasonal climate prediction and improving disaster prevention and mitigation in Eurasia.

## Results

### The NAT pattern in boreal winter and spring

EOF analysis is performed to obtain the dominant modes of interannual variability in the boreal winter (December, January, and February, DJF) and spring (March, April, May, MAM) North Atlantic SST from 1979 to 2018 (Fig. S2). The spatial structures of the main mode of EOF in DJF and MAM show the “negative-positive-negative” meridional pattern, and both passed the test of North et al.<sup>38</sup> We defined the normalized time series as the NAT index (NATI).

We determine a positive and negative NAT based on the normalized 3-month mean NATI. The 0.4 standard deviation is used as the criterion to obtain positive and negative NAT years. Two types of NAT evolutions from DJF to MAM have been identified in the analysis of the NATI (Fig. 1a). In the first type, the NATI displays a switch sign from DJF to MAM (denoted by “PN” and “NP”). The NATI maintains its sign from DJF to MAM in the second type (denoted by “PP” and “NN”). The two NAT SSTA phase evolution types are denoted as transition and persisting, respectively. They are highlighted in green and red colors, respectively, in Fig. 1a. From 1979 to 2018, there are eleven positive (negative) NAT persisting years and five positive-negative (negative-positive) NAT transition years from DJF to MAM.

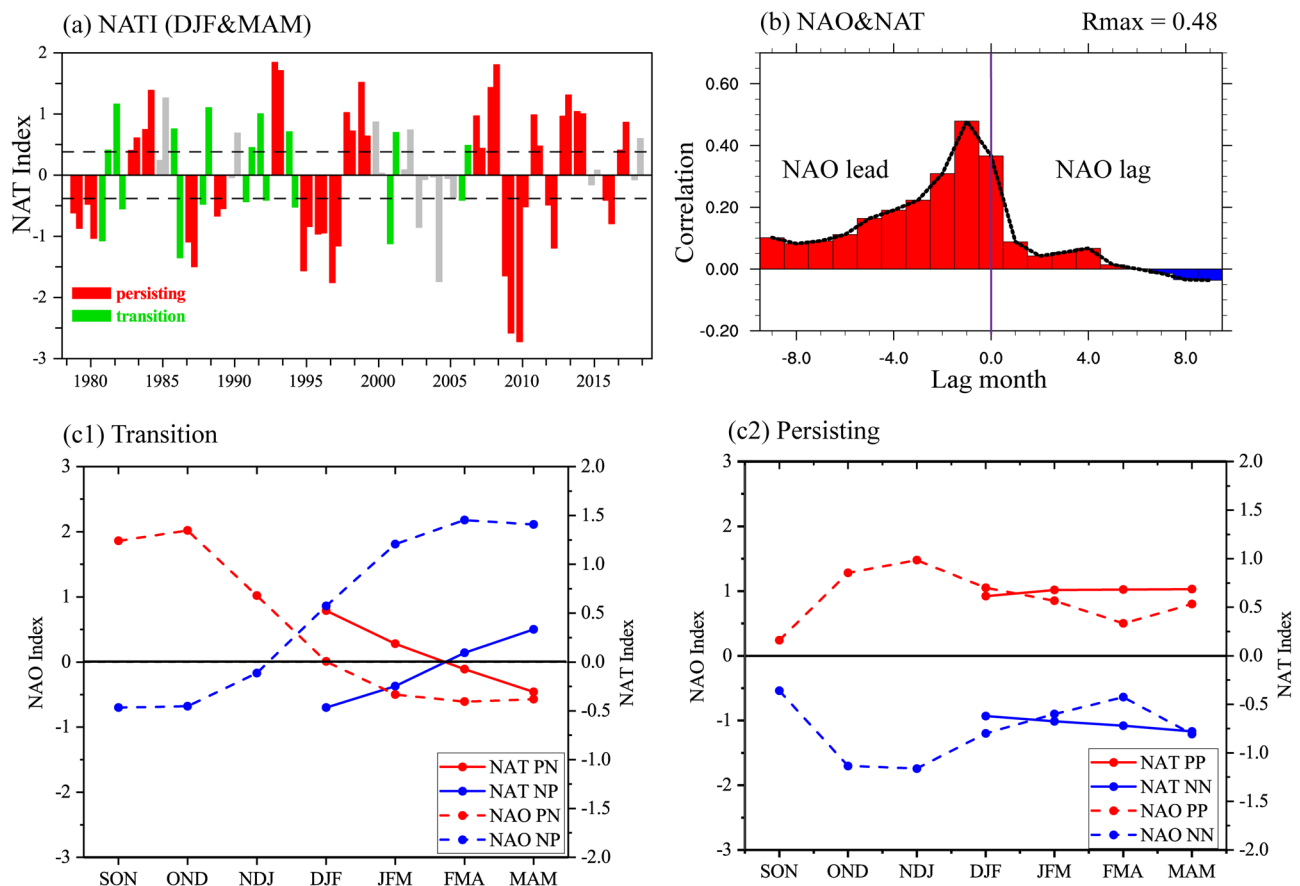


**Fig. 1 | Analysis of NATI variations and correlations with NAOI. a** Normalized NATI in DJF (left bar) and MAM (right bar). Red and green colors denote years with NAT persisting and transition from DJF to MAM. The horizontal dashed lines denote the 0.4 standard deviation. **b** The 9 months lead-lag correlation analysis on

NATI and NAOI. The evolutions of NATI (solid line) and NAOI (dashed line): The NAT persisting years are represented by (c1), while the NAT transition years are represented by (c2).

In addition, we conducted the lead-lag correlation analysis on NATI and NAOI, finding that when NAO is leading 1–3 months, the correlation between NATI and NAOI is high (reaching 0.48), followed by the same period, and both passed the 90% significance test (Fig. 1b). The transition and persisting evolution of NATI and NAOI are provided in Fig. 1c1, c2, suggesting that when the NAT SSTA phase changes, the NAO phase shifts leading 1–3 months earlier; When the NAT SSTA phase persists, the NAO phase also persists. The findings are consistent with the correlation analysis (Fig. 1b). The next section will discuss the specific process and mechanism of the interaction between NAO and NAT.

### Atmospheric forcing on SSTs

We construct composite anomalies of positive minus negative NAT persisting years (PP minus NN) and the positive-negative minus negative-positive NAT transition years (PN minus NP), respectively. Considering that the correlation between NAOI and NATI reaches the highest when NAOI leading 1–3 months (Fig. 1), the analysis of atmospheric circulation (including wind, geopotential height, and sea surface pressure) is leading 1 month in this section. The descriptions in the following refer to the anomalies in the positive NAT SSTA persisting cases and the positive-negative NAT SSTA transition cases.

The NAT phase persisting and transition years display different spatiotemporal evolution of atmospheric circulation and sea surface heat flux anomalies over the North Atlantic. In the NAT phase persisting cases, a tripole pattern of SSTA is maintained from DJF to MAM. This is accompanied by negative SLP anomalies in the high-latitude region and positive SLP anomalies in the mid-latitude region. These anomalies persist from DJF to MAM, displaying a typical positive NAO phase pattern (Fig. 2a1–a4). Correspondingly, the low- and high-level tropospheric geopotential height exhibit negative and positive anomalies in high-latitude and mid-latitude regions, respectively (Fig. 2b1–b4). The westerly wind anomaly increases around 50°N and decreases around 30°N, indicating that the westerly jet core shifts northward and the downstream jet strengthens (Fig. 2c1). In following January to March, the positive NAO pattern is maintained (Fig. 2a2–a4). The low- and high-level tropospheric geopotential height anomalous amplitudes decrease and move northwestward (Fig. 2b2–b4). This is accompanied by westerly wind anomaly persisting increases around 50°N and decreases around 30°N (Fig. 2c2–c4).

The spatiotemporal relationship between wind and SSTA indicates the role of the wind in the SST changes. In particular, wind-related latent heat flux (LHF) and sensible heat flux (SHF) have an important contribution to the SST changes. In the NAT phase persisting cases, anomalous westerlies are in the same direction as climatological mean winds over the high-latitude region and the subtropics (Fig. 2c1–c4). This enhances surface wind speed (WPD) (Fig. 3a1–a4), upward LHF (Fig. 3b1–b4), and upward SHF (Fig. 3c1–c4). The enhanced LHF and SHF contribute to the formation and maintenance of negative SSTA in the mid-latitude and subtropical regions. Along 25°N–40°N, anomalous winds are against climatological mean winds. As such, surface WPD is reduced (Fig. 3a1–a4), suppressing upward LHF (Fig. 3b1–b4) and SHF (Fig. 3c1–c4). These contribute to the formation and maintenance of positive SSTA. In following January to March, WPD, LHF, and SHF anomalies pattern essentially persists. This causes the corresponding upward heat flux to continue decreasing at mid-latitudes, while increasing at high-latitude and subtropical regions, resulting in a positive NAT SSTA phase persisting. Along with surface heat flux, the atmospheric anticyclonic (cyclonic) surface wind stress curl drives northward (southward) oceanic horizontal current in its south flank. Ekman advection is anomalously northward and southward in the south and north of 42°N from DJF to MAM, respectively. They transport warm and cold seawater from lower and higher latitudes to the south and north of 42°N, respectively, resulting in warm and cold SSTAs (Figs. S3b1–S1b4 in Supporting Information S1).

In the NAT phase transition cases, a positive NAT SSTA phase is observed in DJF, but it shifts to a “positive-negative-positive” pattern in MAM (Fig. 4a1–a4). This is accompanied NAO phase shifting from positive

to negative as well (Fig. 4a1–a4). Correspondingly, the low- and high-level tropospheric geopotential height exhibit negative-positive anomalies in high-latitude and mid-latitude regions in NDJ, respectively (Fig. 4b1). However, it shifts to a positive-negative pattern in DJF (Fig. 4b2). The westerly wind anomaly also has the transition (Fig. 4c1–c4). Besides, from January to March, the negative NAO pattern is maintained (Fig. 4a2–a4). The low- and high-level tropospheric geopotential height anomalous amplitudes increase (Fig. 4b2–b4). This is accompanied by westerly wind anomaly persisting decreases around 40°N and increases around 20°N (Fig. 4c2–c4). Figure 5 shows the surface WPD and heat flux anomalies corresponding to NAT phase transition cases. Surface WPD anomalies shift from a positive-negative-positive pattern to a negative-positive-negative pattern in November–March (Fig. 5a1–a4), which leads upward LHF and SHF anomalies shifting from a negative-positive-negative pattern to a positive-negative-positive pattern. This leads to the transition of the NAT SSTA pattern from DJF to MAM (Fig. 4a1–a4). Corresponding to the nearly reversed circulation anomaly, the Ekman flow anomalies turn southward (northward) in the south (north) of 38°N from DJF to MAM, cooling (warming) the SST in the south (north) of 38°N, respectively (Figs. S4b1–b4 in Supporting Information S1). The NAO pattern atmospheric circulation modulates sea surface heat flux and sea surface flow, resulting in the NAT SSTA phase maintaining/transitioning during DJF to MAM.

### Oceanic Feedback on Atmospheric Circulation

The above analysis illustrates the role of wind anomalies induced by the NAO in the North Atlantic SST changes through modulating surface heat fluxes and ocean advection processes. The various wind anomalies are associated with distinct SSTA patterns. In turn, the different SSTA patterns may contribute to the distinct evolution of the atmospheric circulation anomalies. Here, we examine the feedback of the SSTA on the atmosphere by analyzing the Eady growth rate (EGR), extended EP flux (E-P flux), and geopotential tendency anomalies (see details in “Methods”) in the NAT phase persisting and transition years.

Positive EGR anomalies are observed over the mid-latitude North Atlantic in the NAT SSTA phase persisting cases (Fig. 6a1–a4), while the EGR anomalies are almost opposite in NAT SSTA phase transition cases (Fig. 6c1–c4). The E-P flux anomalies also differ between the NAT SSTA phase persisting and transition years. In the NAT phase persisting years, divergent anomalous E-P fluxes are observed around 50°N in the North Atlantic region (Fig. 6b1–b4), suggesting the increased westerly wind anomaly (Wu et al.<sup>14</sup>). In the NAT SSTA phase transition years, convergent anomalous E-P fluxes are observed around 40°N and divergent anomalous E-P fluxes are seen around 25°N in the North Atlantic region (Fig. 6d1–d4), suggesting the increased westerly wind anomaly around 25°N and decreased westerly wind anomaly around 30°N. The above results signify the feedback of the synoptic-scale eddy activities on the low-frequency mean flow. Anomalous synoptic-scale activities and EP flux indicate that the NAT SSTAs generate positive feedback on the NAO-type wind anomaly pattern in the NAT SSTA phase persisting/transition cases.

Figure 7 shows the EV flux-induced and eddy heat forcing (EH) flux-induced geopotential height anomalies over the North Atlantic. EH forcing results in an atmospheric baroclinic response in the vertical direction (Fig. 7b1–b4), while EV forcing leads to an equivalent barotropic response (Fig. 7a1–a4). In the NAT SSTA phase persisting cases, the EV flux generates positive feedback to the positive NAO phase throughout the troposphere, which is notably stronger in the upper troposphere compared to the middle–lower troposphere (Fig. 7a1–a4). The EH flux generates positive (negative) geopotential height forcing in the upper troposphere and negative (positive) forcing in the lower troposphere over the 35°N–45°N (45°N–60°N) North Atlantic region. Therefore, the EH flux-induced forcing negatively feeds back to positive NAO phase flow in the upper troposphere and positively feeds back to positive NAO phase flow in the lower troposphere (Fig. 7b1–b4). However, the forcing is smaller in magnitude than the EV flux-induced forcing. In the NAT SSTA phase transition cases, the eddy-induced geopotential height anomalies are almost opposite (Fig. 8). As a



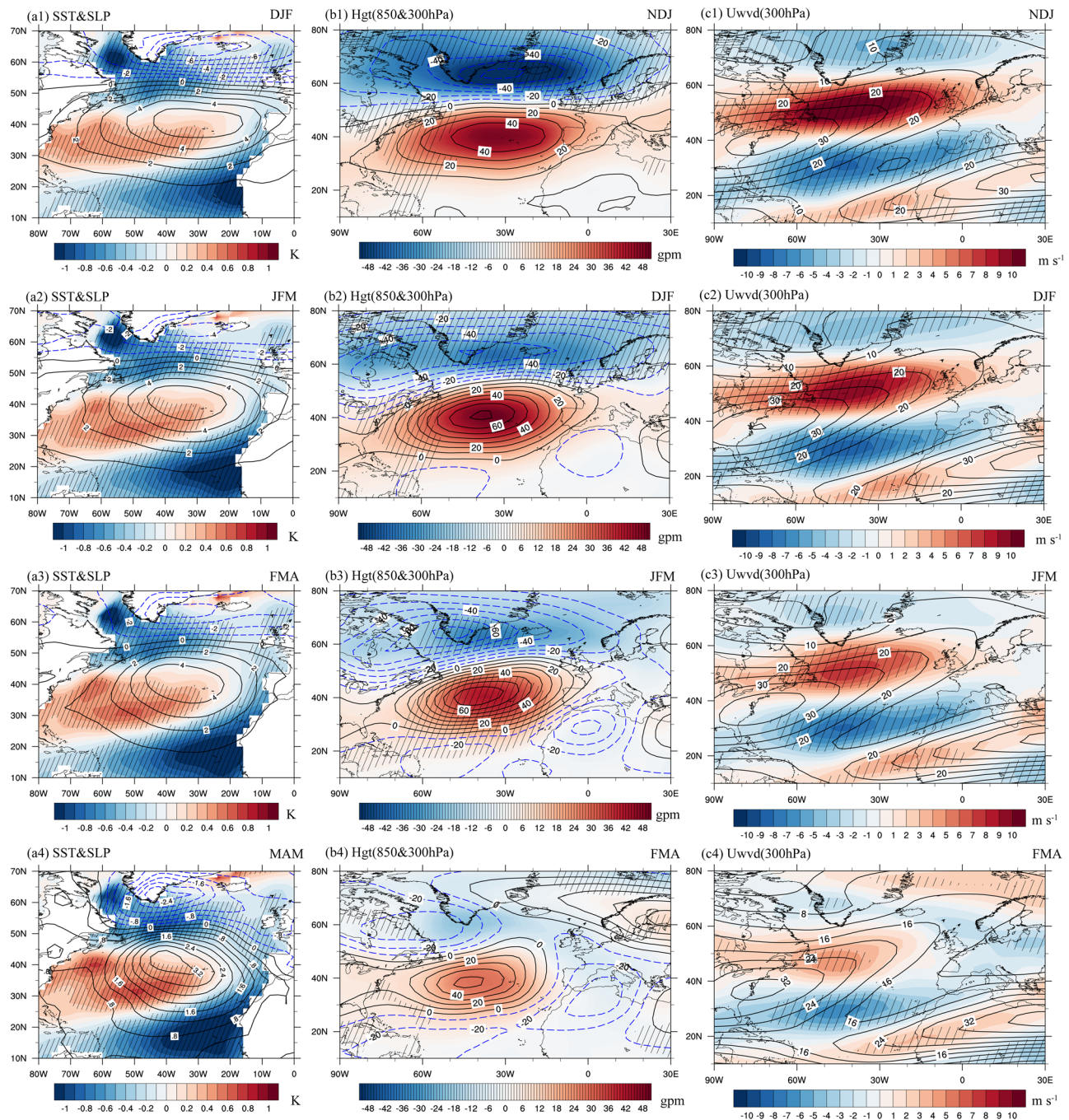


**Fig. 2 | Month-by-month evolutions of SSTA and Atmospheric circulation anomalies in persistent years.** SSTA (colors in **a1–a4**, units: K) from DJF to MAM, and SLP (contours in **a1–a4**, units: hPa), 850 hPa (colors in **b1–b4**, units: gpm) and 300 hPa geopotential height (contours in **b1–b4**, units: gpm), 300 hPa zonal wind (colors in **c1–c4**, units:  $\text{m s}^{-1}$ ) anomalies from NDJ to FMA in persisting years. The

contours in (**c1–c4**) denote the corresponding climatological zonal wind. The corresponding abbreviated month name is labeled in the top-right corner of each panel. The black slashes indicate the colored regions exceeding 90% confidence level with the Student's *t*-test.

result, in the NAT SST phase persisting/transition cases, NAT SSTs actively feedback upon the positive/negative NAO phase atmospheric circulation through eddy forcing.

## Discussion

The present study identifies two distinct evolutions of the NAT SSTA phase from DJF to MAM: the NAT SSTA phase persisting and switching. The physical mechanism of NAT SSTA phases persistence or transition from boreal winter to spring is revealed and the relationship between NAO and NAT SSTA is examined. The results indicate that the North

Atlantic air-sea coupling is critical for the maintenance/transition of the NAT SSTA phase from DJF to MAM. The NAO-related wind anomalies generate the evolutions of the NAT SSTA phase mainly through wind-related surface heat flux. In turn, the NAT SSTA provides positive feedback for the maintenance of the former NAO pattern through the eddy-mean flow interaction. To better understand the mechanisms, we establish a schematic diagram summarizing the role of air-sea coupling in the evolution of the NAT SSTA phase from DJF to MAM in Fig. 9. In the NAT SSTA phase persisting cases, the positive-phase NAO is maintained, resulting in increased westerly around 50°N and a spatial distribution of “



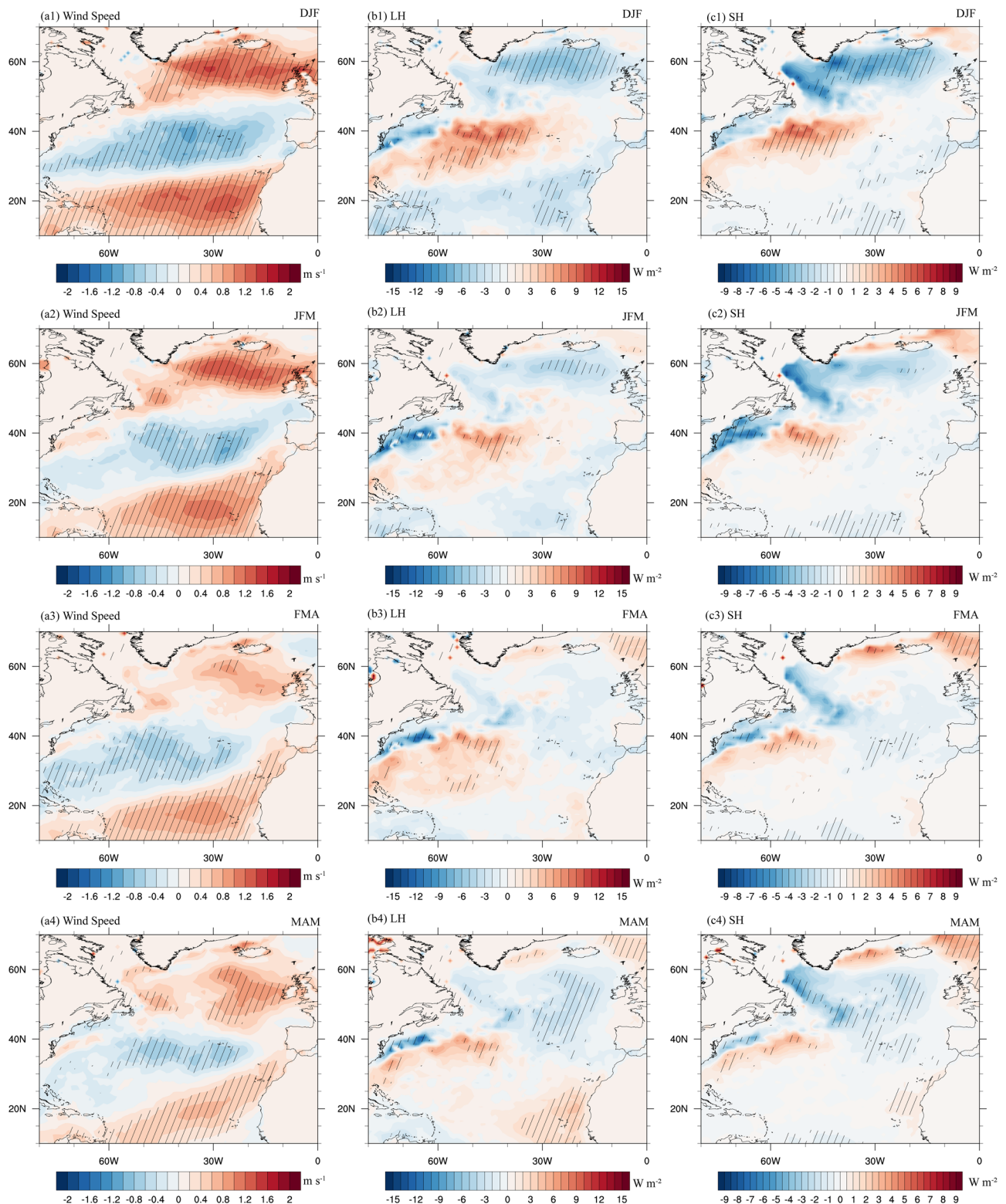


**Fig. 3 | Month-by-month evolutions of surface wind speed and heat flux anomalies in persistent years.** Surface wind speed (WPD) (colors in **a1–a4**, units:  $\text{m s}^{-1}$ ), LHF (colors in **b1–b4**, units:  $\text{W m}^{-2}$ ), and SHF (colors in **c1–c4**, units:  $\text{W m}^{-2}$ ) anomalies from DJF to MAM in persisting years. The corresponding

abbreviated month name is labeled in the top-right corner of each panel. The black slashes indicate the colored regions exceeding 90% confidence level with the Student's *t*-test.

positive-negative-positive “ for surface WPD. This leads to a spatial distribution of “negative-positive-negative” for surface heat flux anomalies and maintains the positive-phase NAT SSTA from DJF to MAM (Fig. 9a1). The sustained SSTA induces atmospheric baroclinic instability

near 50°N, which in turn generates positive feedback on the positive-phase NAO circulation by forcing cyclonic vorticity to the north and anticyclonic vorticity to the south (Fig. 9a2). In contrast, in NAT SSTA phase transition cases, there is a shift from positive to negative of the NAO phase

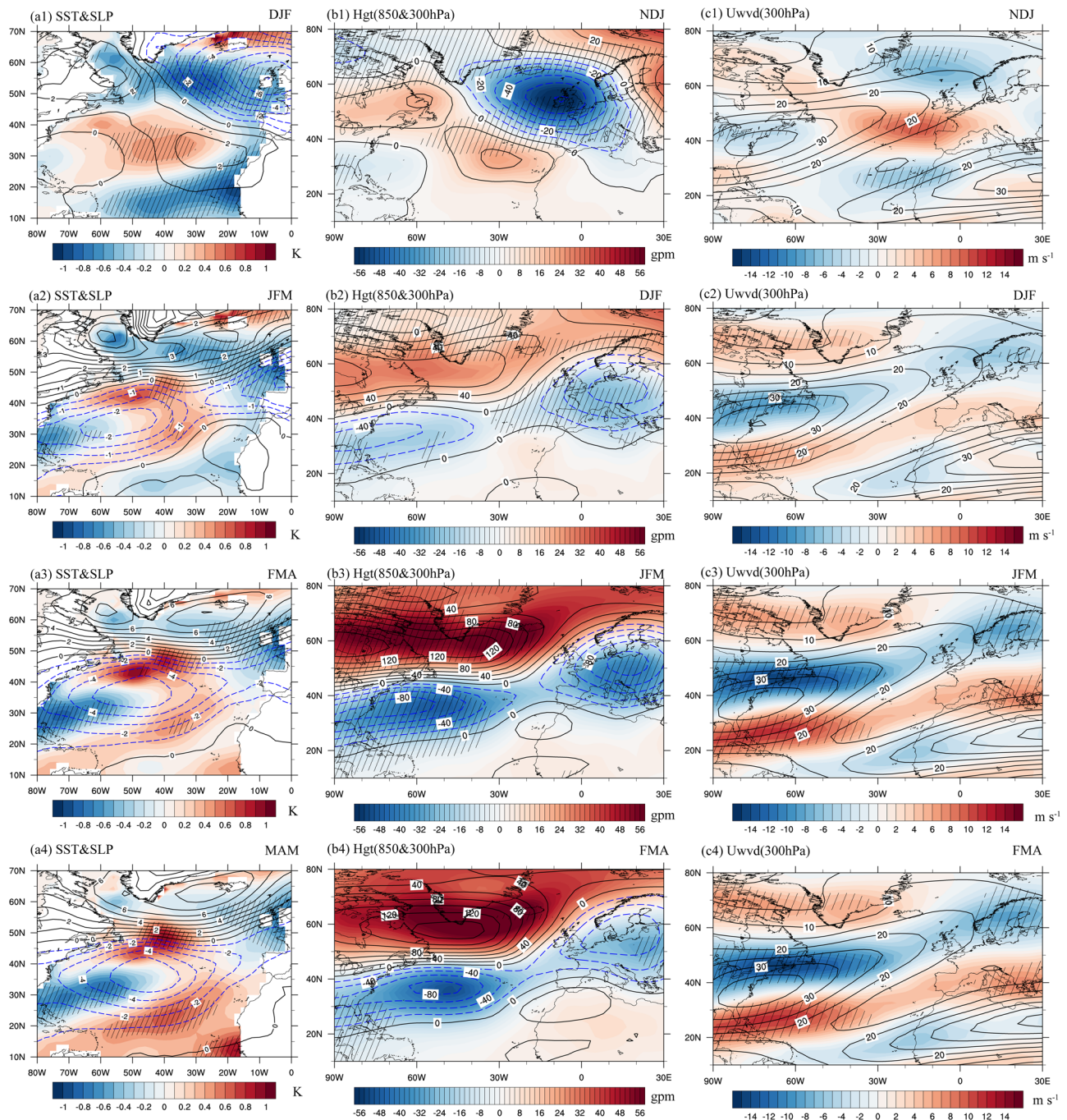


**Fig. 4 | Month-by-month evolutions of SSTA and Atmospheric circulation anomalies in transition years.** SST (colors in **a1–a4**, units: K) anomalies from DJF to MAM, and SLP (contours in **a1–a4**, units: hPa), 850 hPa (colors in **b1–b4**, units: gpm) and 300 hPa geopotential height (contours in **b1–b4**, units: gpm), 300 hPa zonal wind (colors in **c1–c4**, units:  $\text{m s}^{-1}$ ) anomalies from NDJ to FMA in transition

years. The contours in (**c1–c4**) denote the corresponding climatological zonal wind. The corresponding abbreviated month name is labeled in the top-right corner of each panel. The black slashes indicate the colored regions exceeding 90% confidence level with the Student's *t*-test.

from NDJ to DJF. This transition is associated with reversed WPD and heat flux anomalies that drive the change in the NAT SSTA phase (Fig. 9b1). The transitional SSTA also generates positive feedback on the negative-phase NAO through transient eddy activities (Fig. 9 b2). Our analysis suggests that the change of the NAO phase is leading 1–3 months for the NAT SSTA phase. When the phase of NAO persists (switches) during NDJ–DJF, the NAO-driven atmospheric circulation favors the maintenance (transition) of the NAT SSTA phase from winter through spring (Table 1). Weather and climate anomaly patterns over Eurasia are

highly dependent upon the phase of the NAT SSTA<sup>39,40</sup>. The change in the NAT SSTA phase signifies that the NAT-related weather and climate anomalies may not be steady from boreal winter to spring. However, due to the slow changes in SST, the previous predictions of summer precipitation have assumed that the NAT SSTA phase persists from DJF to MAM. This assumption may lead to inaccurate predictions when the NAT SSTA phase changes. Our research offers a new criterion for predicting summer climate in Eurasia, which is important for NAT-related climate predictability.



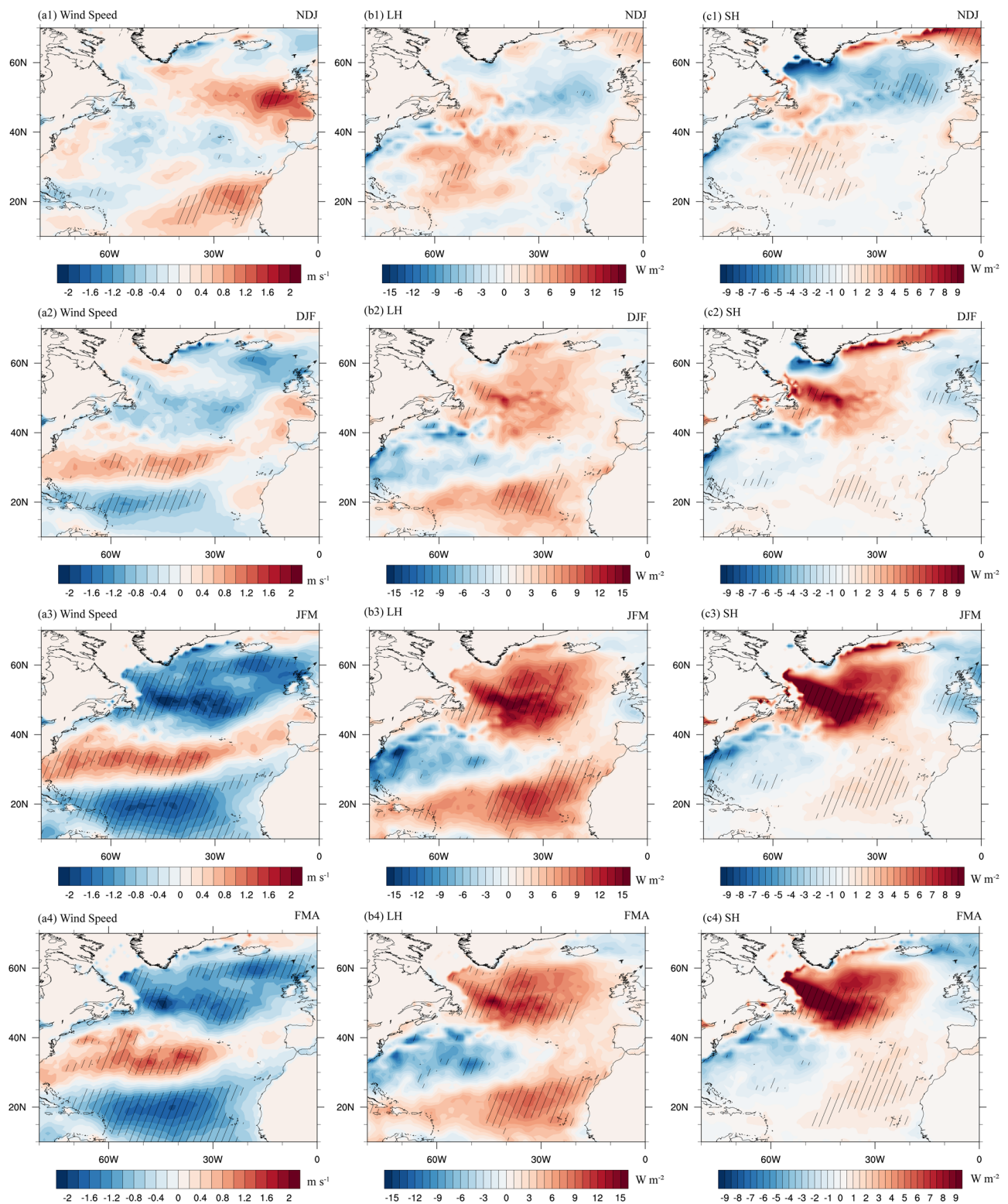


**Fig. 5 | Month-by-month evolutions of surface wind speed and heat flux anomalies in transition years.** Surface WPD (colors in **a1–a4**, units:  $\text{m s}^{-1}$ ), LHF (colors in **b1–b4**, units:  $\text{W m}^{-2}$ ), and SHF (colors in **c1–c4**, units:  $\text{W m}^{-2}$ ) anomalies

from NDJ to FMA in transition years. The corresponding abbreviated month name is labeled in the top-right corner of each panel. The black slashes indicate the colored regions exceeding 90% confidence level with the Student's *t*-test.

This study primarily examines the mechanisms behind the persistence and transition of the NAT SSTA phase, focusing on the interaction between the NAO and NAT. However, the factors influencing the NAT SSTA phase are complex and varied. On the interdecadal scale, the Atlantic Multi-decadal Oscillation (AMO) plays a significant role in regulating interdecadal

global climate variations<sup>41–43</sup>. The interannual relationship between NAO and NAT is significantly influenced by the AMO phase, with a stronger association between them during the periods of the 1950s–1960s and after the mid-1990s but weaker during the 1970s–1980s<sup>24,44,45</sup>. As the influence of the NAO on NAT SSTA may depend on the intensity of NAO and the phase



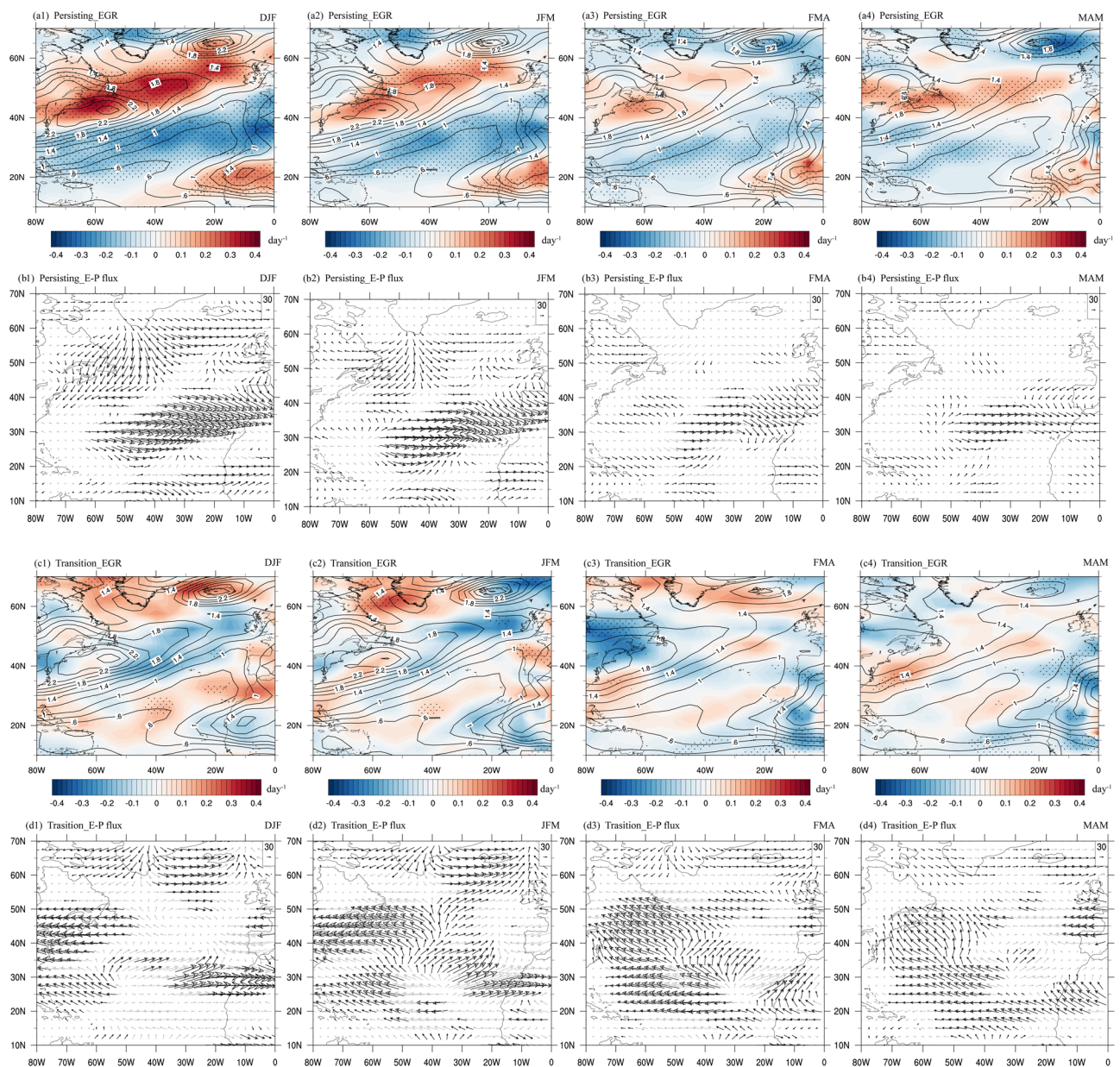


**Fig. 6 | Month-by-month evolutions of EGR and E-P flux anomalies at 850 hPa from DJF to MAM.** EGR anomalies (colors in **a1–a4**, units:  $\text{day}^{-1}$ ) and E-P flux anomalies (vectors in **b1–b4**, units:  $\text{m}^2 \text{s}^{-2}$ ) in the NAT SSTA phase persisting years. **c1–c4** and **d1–d4** are same as **a1–a4** and **b1–b4**, but in the transition year. The

contours denote the corresponding climatological EGR. The corresponding abbreviated month name is labeled in the top-right corner of each panel. The black dots (vectors) indicate the colored regions (E-P flux anomalies) exceeding 90% confidence level with the Student's t-test.

of AMO, an interesting question is how changes in the relationship between the NAO and NAT SSTA on an interdecadal timescale. The role played by AMO in this connection needs to be further explored through diagnostic analysis and numerical model simulation in the future.

On the other hand, as the dominant climate mode on the interannual time scale, ENSO is suggested to significantly impact the NAT SSTA, NAO and extratropical jet streams through the poleward and eastward propagation of Rossby wave and interaction with the extratropical winter stratosphere<sup>46–49</sup>. Previous studies have shown discrepancies regarding the role of ENSO in NAO variability. Some researches indicated that ENSO may induce a reversal of the NAO phase from early winter to late winter<sup>50–53</sup>. While others studies reveal that the NAO may maintain its phase across winter during both ENSO and normal years<sup>14</sup>. Besides, the ENSO has a delayed effect on NAO/AO, and this behavior is a result of migrating atmospheric angular momentum anomalies<sup>54</sup>. In this study, the primary effect of ENSO has been linearly removed. Whether ENSO plays a role in the

evolution of the NAT SSTA phase and what role it plays? This needs to be further studied.

Moreover, the atmosphere (including wind and heat flux) tends to drive the North Atlantic SST variations on the interannual timescales. On the decadal timescales, oceanic processes (including the combined effect of ocean circulation and vertical mixing) tend to drive the SSTAs that in turn influence the air-sea heat exchange<sup>55</sup>. Our study primarily discussed the influence of turbulent heat fluxes on driving the NAT SSTA, while active ocean processes were not fully considered. The influence of ocean processes on the NAT SSTA phase evolution is also a key area for our future research.

## Methods

### Data

Monthly SST data on a horizontal resolution of  $2^\circ \times 2^\circ$  are derived from the National Oceanic and Atmospheric Administration (NOAA) Extended Reconstructed SST version 5 (ERSSTv5) dataset<sup>56</sup>. Atmospheric circulation

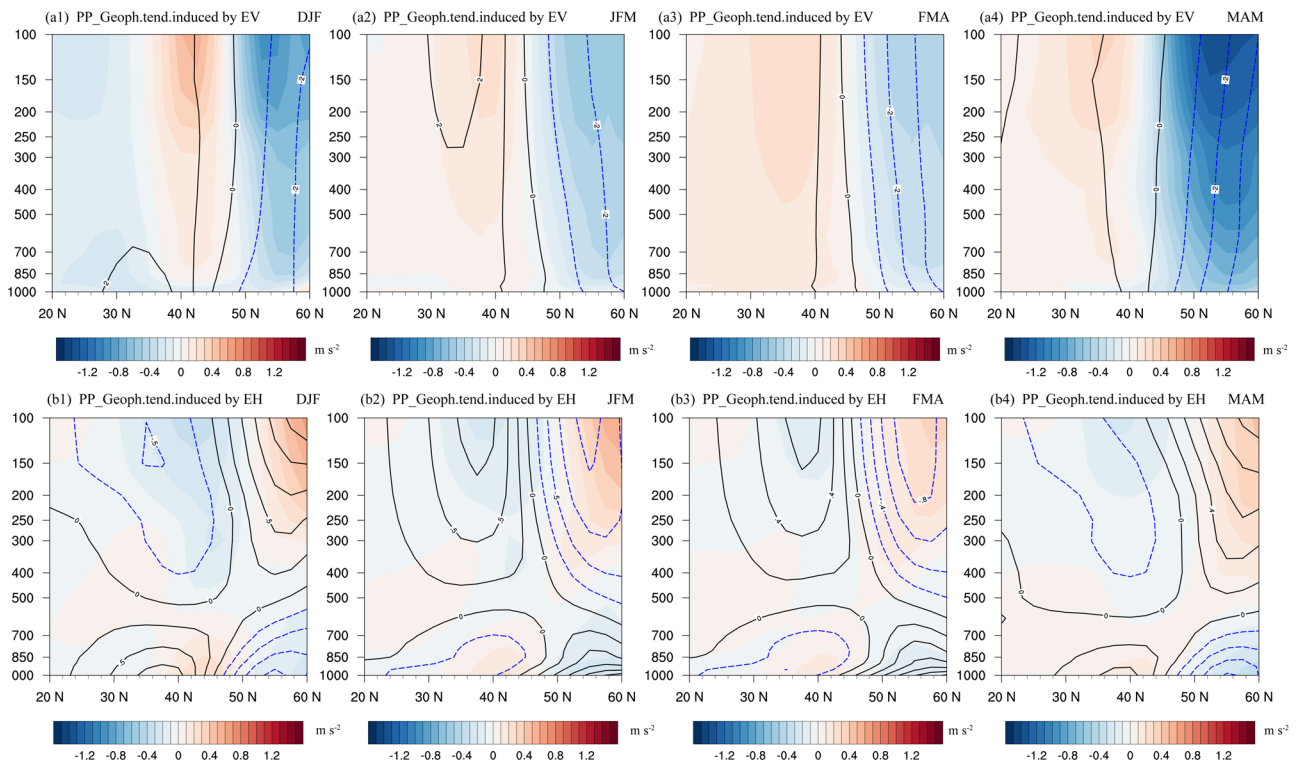


**Fig. 7 | Latitude-altitude sections averaged between 60°W and 0° of eddy-induced geopotential tendency in persisting years.** EV (a1–a4, units:  $10^{-4} \text{ m s}^{-2}$ ) and EH (b1–b4, units:  $10^{-4} \text{ m s}^{-2}$ ) induced geopotential tendency from DJF to MAM. The

contours in (a1–a4, b1–b4) denote their corresponding climatology, respectively. The corresponding abbreviated month name is labeled in the top-right corner of each panel.

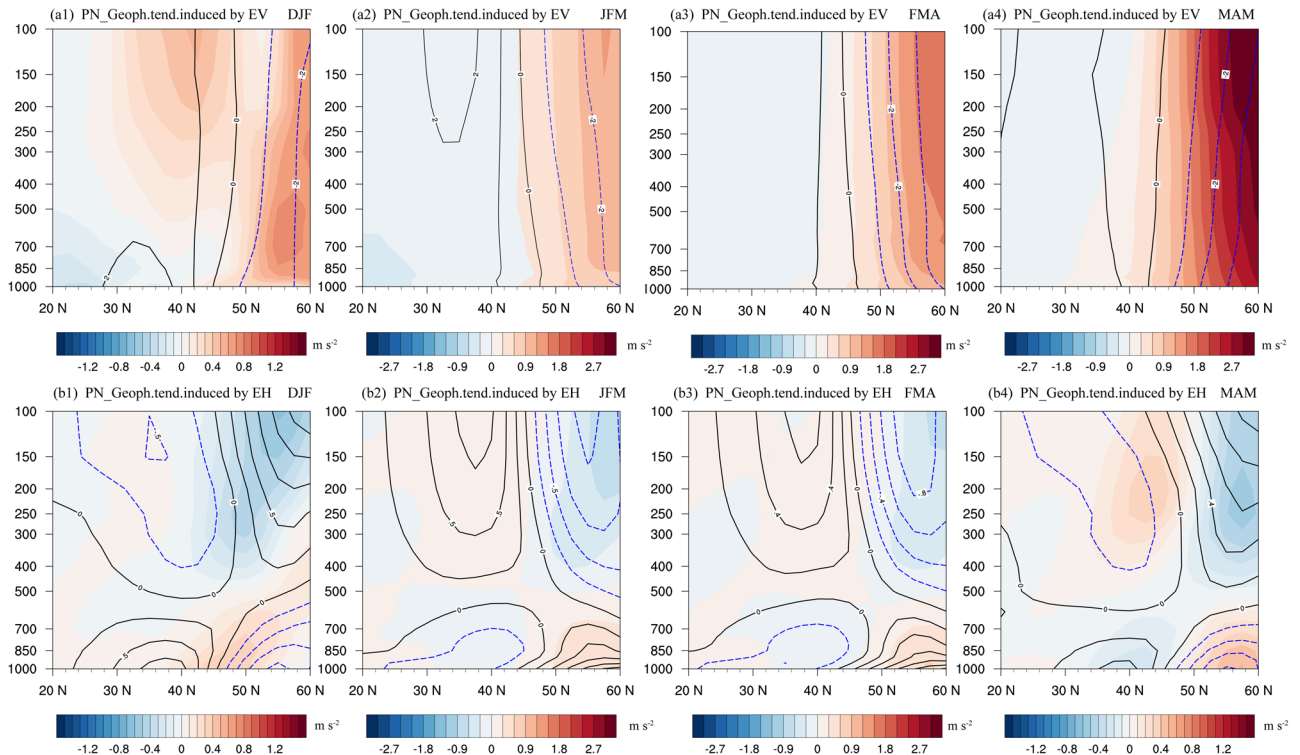
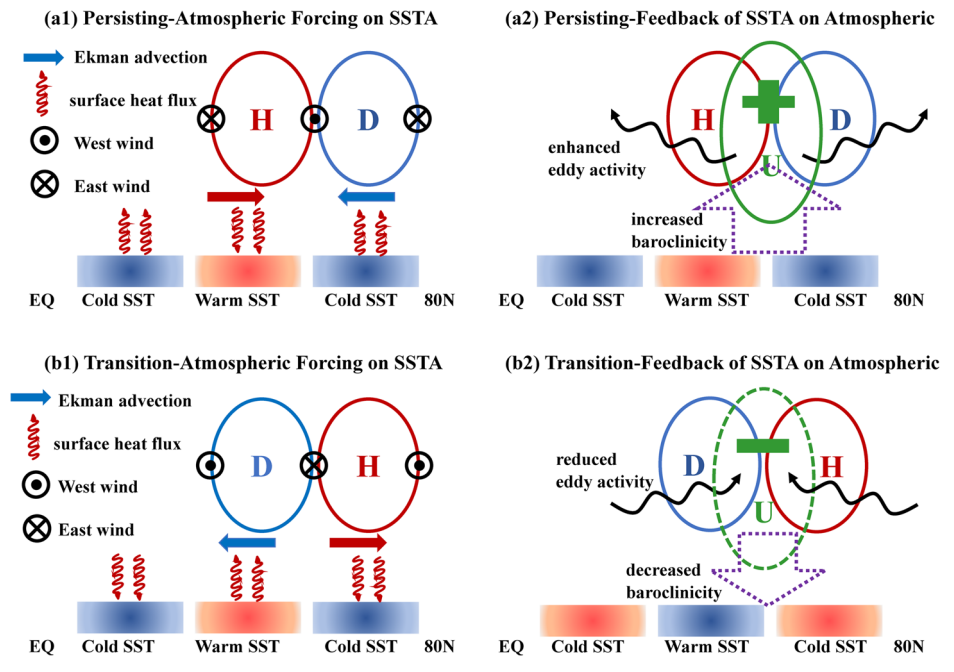


**Fig. 8 | Latitude-altitude sections averaged between 60°W and 0° of eddy-induced geopotential tendency in transition years.** EV (a1–a4, units:  $10^{-4} \text{ m s}^{-2}$ ) and EH (b1–b4, units:  $10^{-4} \text{ m s}^{-2}$ ) induced geopotential tendency from DJF to MAM. The

contours in (a1–a4, b1–b4) denote their corresponding climatology, respectively. The corresponding abbreviated month name is labeled in the top-right corner of each panel.

**Fig. 9 | Schematic diagrams describing mechanisms of the NAT SSTA phase changes from DJF to MAM. a1, a2** are the processes of atmospheric forcing on SSTAs and oceanic feedback on atmospheric circulation in the NAT SSTA phase persisting case. **b1, b2** are same as **(a1, a2)**, but for NAT SSTA phase transition case. The red (blue) shaded area denotes the warm (cold) SSTA; the solid red (dashed blue) circle indicates the positive (negative) geopotential height anomaly; The solid blue (red) arrow denotes the cold (warm) advection; the dashed purple arrow denotes increased/decreased atmospheric baroclinicity.



fields including the winds, vertical velocity, sea level pressure (SLP), and so on are obtained from the National Centers for Environmental Prediction/National Center for Atmospheric Research (NCEP/NCAR) Reanalysis on a  $2.5^\circ \times 2.5^\circ$  horizontal resolution<sup>57</sup>. We also used the Objectively Analyzed air-sea Fluxes (OAFlux) dataset<sup>58</sup> to analyze the surface heat flux over the North Atlantic.

### Statistical tools and significance

EOF and composite methods are employed in this study. To focus on the interannual variability, the interdecadal component (the 9-yr running mean) is removed before all the calculations. Additionally, the ENSO significantly impacts the interannual variations of the mid-high-latitude atmospheric circulation. The correlation coefficient between monthly NATI and NINO3.4 index reached  $-0.16$  (over 99% significance test). Therefore, we linearly removed ENSO signals from the SST and circulation fields by subtracting the regressions on the standardized Niño 3.4 index<sup>59</sup>. A two-tailed Student's *t*-test is used for determining statistical significance.

### The simplified 3-D quasi-geostrophic potential vorticity equation

To examine the contributions of transient synoptic eddy forcing to the low-frequency flow, we adopt the approach outlined by Lau and Holopainen<sup>60</sup>. The simplified 3-D quasi-geostrophic potential vorticity equation could be written as follows:

$$\left[ \frac{1}{f} \nabla^2 + f \frac{\partial}{\partial p} \left( \frac{1}{\sigma_1} \frac{\partial}{\partial p} \right) \right] \left( \frac{\partial \Delta \phi}{\partial t} \right) = D^{VORT} + D^{HEAT} + R_1 \quad (1)$$

$$D^{VORT} = -\nabla \cdot \bar{\vec{V}}_h' \zeta' \quad (2)$$

$$D^{HEAT} = f \frac{\partial}{\partial p} \left( \frac{\nabla \cdot \bar{\vec{V}}_h' \theta'}{\bar{S}} \right) \quad (3)$$

where  $f$  denotes the Coriolis parameter,  $\phi$  is the geopotential,  $\sigma_1$  is the atmospheric static stability parameter ( $\sigma_1 = -a \cdot \partial \ln \theta / \partial p$ ),  $a$  is the specific volume,  $T$  is the temperature,  $\Delta$  denotes the anomaly, and overbar denotes the monthly mean. The term  $R_1$  in Eq. (1) represents all remaining components in the quasi-geostrophic potential vorticity balance.  $D^{VORT}$  and  $D^{HEAT}$  represent the eddy-induced vorticity (EV) and heat forcing (EH).  $\bar{S}$  is

**Table 1 | The criteria for NAT SSTA phase persistence and transition from DJF to MAM**

Evolutions	Criteria			Results
	NAO (NDJ)	NAO (DJF)	NAT (DJF)	NAT (MAM)
Persistence	Positive (+)	Positive (+)	Positive (+)	Positive (+)
	Negative (−)	Negative (−)	Negative (−)	Negative (−)
Transition	Positive (+)	Negative (−)	Positive (+)	Negative (−)
	Negative (−)	Positive (+)	Negative (−)	Positive (+)

the hemispheric mean of the quantity  $-\partial \theta / \partial p$ .  $\bar{\vec{V}}_h'$ ,  $\zeta'$  and  $\theta'$  represent the 2–8-day filtered horizontal wind vector, relative vorticity, and potential temperature.

To individually examine the 3D geopotential tendency induced by EV and EH, this equation can be solved by inserting the forcing terms  $D^{VORT}$  and  $D^{HEAT}$  separately. Given the forcing terms, the tendency of geopotential height anomalies can be numerically solved with the successive over-relaxation (SOR) method. The settings of boundary conditions are important and may disturb the solution as the SOR method is applied<sup>61</sup>.

### Eady growth rate

The atmospheric baroclinicity is represented by Eady growth rate ( $\sigma_{BI}$ ), calculated using the formula<sup>62</sup>:

$$\sigma_{BI} = 0.31 \frac{f}{N} \left| \frac{\partial U}{\partial z} \right| \quad (4)$$

where  $N$  is the Brunt-Väisälä frequency,  $U$  is the horizontal wind speed, and  $z$  is the vertical potential height. The low-level atmospheric baroclinicity is closely related to high-frequency transient eddy activity<sup>62</sup>.

### The extended E-P flux

The extended E-P flux<sup>63–66</sup> is used for estimating the dynamical interaction between low-frequency mean flow and synoptic-scale eddy activity. Following Trenberth<sup>66</sup>, the horizontal component of the extended E-P flux is



calculated as follows:

$$E = \left[ \frac{1}{2} \times (\sqrt{v^2 - u^2}) \vec{i}, -\vec{v} \right] \times \cos \varphi \quad (5)$$

where  $\varphi$ ,  $u'$  and  $v'$  indicate the latitude, and synoptic-scale zonal and meridional winds, respectively. Synoptic-scale wind variations on the 2–8-day timescale are obtained through a band-pass Lanczos filter applied to the original daily winds.

## Data availability

The National Oceanic and Atmospheric Administration (NOAA) Extended Reconstructed sea surface temperature version 5 dataset (ERSST.v5) can be obtained from <https://psl.noaa.gov/data/gridded/data.noaa.ersst.v5.html>. The Nino 3.4 index is available at [psl.noaa.gov/gcos\\_wgsp/Timeseries/Nino34/](https://psl.noaa.gov/gcos_wgsp/Timeseries/Nino34/). The NAO index was obtained from <https://climatedataguide.ucar.edu/climate-data/hurrell-north-atlantic-oscillation-nao-index-station-based>. The NCEP monthly mean reanalysis data are available at <https://psl.noaa.gov/data/gridded/data.ncep.reanalysis.derived.html>. The OAFUX data set was downloaded from <https://rda.ucar.edu/datasets/ds260.1/dataaccess/>.

## Code availability

The NCL codes used to run the analysis can be obtained upon request from the corresponding authors.

Received: 19 September 2024; Accepted: 17 December 2024;

Published online: 24 December 2024

## References

- Enfield, D. B., Mestas-Núñez, A. M. & Trimble, P. J. The Atlantic Multidecadal Oscillation and its relation to rainfall and river flows in the continental US. *Geophys. Res. Lett.* **28**, 2077–2080 (2001).
- Sutton, R. T. & Hodson, D. L. R. Climate response to basin-scale warming and cooling of the North Atlantic Ocean. <https://doi.org/10.1175/JCLI4038.1> (2007).
- Zuo, J., Li, W., Sun, C., Xu, L. & Ren, H.-L. Impact of the North Atlantic sea surface temperature tripole on the East Asian summer monsoon. *Adv. Atmos. Sci.* **30**, 1173–1186 (2013).
- Wu, R. et al. Northeast China summer temperature and North Atlantic SST. *J. Geophys. Res. Atmos.* **116**, D16116 (2011).
- Liu, Y., Wang, L., Zhou, W. & Chen, W. Three Eurasian teleconnection patterns: spatial structures, temporal variability, and associated winter climate anomalies. *Clim. Dyn.* **42**, 2817–2839 (2014).
- Chen, S., Wu, R. & Liu, Y. Dominant modes of interannual variability in Eurasian surface air temperature during boreal spring. <https://doi.org/10.1175/JCLI-D-15-0524.1> (2016).
- Gong, H., Wang, L., Chen, W. & Wu, R. Attribution of the East Asian winter temperature trends during 1979–2018: role of external forcing and internal variability. *Geophys. Res. Lett.* **46**, 10874–10881 (2019).
- Chen, S., Wu, R., Chen, W., Hu, K. & Yu, B. Structure and dynamics of a springtime atmospheric wave train over the North Atlantic and Eurasia. *Clim. Dyn.* **54**, 5111–5126 (2020).
- Kucharski, F., Bracco, A., Yoo, J. H. & Molteni, F. Low-frequency variability of the Indian monsoon–ENSO relationship and the tropical Atlantic: the “weakening” of the 1980s and 1990s. <https://doi.org/10.1175/JCLI4254.1> (2007).
- Kucharski, F. et al. A Gill–Matsuno-type mechanism explains the tropical Atlantic influence on African and Indian monsoon rainfall. *Quart. J. R. Meteor. Soc.* **135**, 569–579 (2009).
- Hong, C., Chang, T. & Hsu, H. Enhanced relationship between the tropical Atlantic SST and the summertime western North Pacific subtropical high after the early 1980s. *J. Geophys. Res. Atmos.* **119**, 3715–3722 (2014).
- Wettstein, J. J. & Wallace, J. M. Observed patterns of month-to-month storm-track variability and their relationship to the background flow. <https://doi.org/10.1175/2009JAS3194.1> (2010).
- Woollings, T. et al. Blocking and its response to climate change. *Curr. Clim. Chang. Rep.* **4**, 287–300 (2018).
- Wu, R., Dai, P. & Chen, S. Persistence or Transition of the North Atlantic Oscillation Across Boreal Winter: Role of the North Atlantic Air–Sea Coupling. *J. Geophys. Res. Atmos.* **127**, e2022JD037270 (2022).
- Hurrell, J. W. Decadal trends in the North Atlantic Oscillation: regional temperatures and precipitation. *Science* **269**, 676–679 (1995).
- Deser, C. & Timlin, M. S. Atmosphere–ocean interaction on weekly timescales in the North Atlantic and Pacific. *J. Clim.* **10**, 393–408 (1997).
- Czaja, A. & Frankignoul, C. Observed impact of Atlantic SST anomalies on the North Atlantic Oscillation. *J. Clim.* **15**, 606–623 (2002).
- Fang, J. & Yang, X.-Q. Structure and dynamics of decadal anomalies in the wintertime midlatitude North Pacific ocean–atmosphere system. *Clim. Dyn.* **47**, 1989–2007 (2016).
- Marshall, J. et al. North Atlantic climate variability: phenomena, impacts and mechanisms. *Int. J. Climatol.* **21**, 1863–1898 (2001).
- Yao, Y., Zhong, Z., Yang, X.-Q. & Lu, W. An observational study of the North Pacific storm-track impact on the midlatitude oceanic front. *J. Geophys. Res. Atmos.* **122**, 6962–6975 (2017).
- Tang, X. & Li, J. Synergistic effect of boreal autumn SST over the tropical and South Pacific and winter NAO on winter precipitation in the southern Europe. *npj Clim. Atmos. Sci.* **7**, 78 (2024).
- Qiu, B. Interannual variability of the Kuroshio Extension system and its impact on the wintertime SST field. *J. Phys. Oceanogr.* **30**, 1486–1502 (2000).
- Tao, L., Fang, J., Yang, X.-Q., Sun, X. & Cai, D. Midwinter reversal of the atmospheric anomalies caused by the North Pacific mode-related Air–Sea coupling. *Geophys. Res. Lett.* **49**, e2022GL100307 (2022).
- Peng, S., Robinson, W. A. & Li, S. Mechanisms for the NAO responses to the North Atlantic SST tripole. *J. Clim.* **16**, 1987–2004 (2003).
- Rodwell, M. J., Rowell, D. P. & Folland, C. K. Oceanic forcing of the wintertime North Atlantic Oscillation and European climate. *Nature* **398**, 320–323 (1999).
- Nie, Y., Ren, H.-L. & Zhang, Y. The role of extratropical air–sea interaction in the autumn subseasonal variability of the North Atlantic Oscillation. *J. Climate* **32**, 7697–7712 (2019).
- Kushnir, Y. et al. Atmospheric GCM response to extratropical SST anomalies: synthesis and evaluation\*. *J. Clim.* **15**, 2233–2256 (2002).
- Li, Z. X. & Conil, S. Transient response of an atmospheric GCM to North Atlantic SST anomalies. *J. Clim.* **16**, 3993–3998 (2003).
- Sein, D. V. et al. The relative influence of atmospheric and oceanic model resolution on the circulation of the North Atlantic Ocean in a coupled climate model. *J. Adv. Model. Earth Syst.* **10**, 2026–2041 (2018).
- Tao, L., Sun, X. & Yang, X. The asymmetric atmospheric response to the midlatitude North Pacific SST anomalies. *J. Geophys. Res. Atmos.* **124**, 9222–9240 (2019).
- Hartmann, D. L. & Lo, F. Wave-driven zonal flow vacillation in the Southern Hemisphere. *J. Atmos. Sci.* **55**, 1303–1315 (1998).
- Herceg-Bulić, I. & Kucharski, F. North Atlantic SSTs as a link between the wintertime NAO and the following spring climate. <https://doi.org/10.1175/JCLI-D-12-00273.1> (2014).
- Han, Z., Luo, F. & Wan, J. The observational influence of the North Atlantic SST tripole on the early spring atmospheric circulation. *Geophys. Res. Lett.* **43**, 2998–3003 (2016).
- Limpasuvan, V. & Hartmann, D. L. Wave-maintained annular modes of climate variability\*. *J. Clim.* **13**, 4414–4429 (2000).
- Wen, N., Liu, Z., Liu, Q. & Frankignoul, C. Observed atmospheric responses to global SST variability modes: a unified assessment using GEFA\*. *J. Clim.* **23**, 1739–1759 (2010).

36. Magnusdottir, G., Deser, C. & Saravanan, R. The effects of North Atlantic SST and sea ice anomalies on the winter circulation in CCM3. Part I: main features and storm track characteristics of the response. *J. Clim.* **17**, 857–876 (2004).
37. Wills, S. M., Thompson, D. W. J. & Ciaso, L. M. On the observed relationships between variability in Gulf Stream sea surface temperatures and the atmospheric circulation over the North Atlantic. <https://doi.org/10.1175/JCLI-D-15-0820.1> (2016).
38. North, G. R., Bell, T. L., Cahalan, R. F. & Moen, F. J. Sampling errors in the estimation of empirical orthogonal functions. *Mon. Weather Rev.* **110**, 699–706 (1982).
39. Chen, S., Wu, R. & Chen, W. Influence of North Atlantic sea surface temperature anomalies on springtime surface air temperature variation over Eurasia in CMIP5 models. *Clim. Dyn.* **57**, 2669–2686 (2021).
40. Cheng, S. et al. Impact of Summer North Atlantic Sea Surface Temperature Tripole on Precipitation over Mid-high-latitude Eurasia. <https://doi.org/10.1175/JCLI-D-24-0072.1> (2024).
41. Sutton, R. T. & Dong, B. Atlantic Ocean influence on a shift in European climate in the 1990s. *Nat. Geosci.* **5**, 788–792 (2012).
42. Li, L., Li, W. & Barros, A. P. Atmospheric moisture budget and its regulation of the summer precipitation variability over the Southeastern United States. *Clim. Dyn.* **41**, 613–631 (2013).
43. Steinman, B. A., Mann, M. E. & Miller, S. K. Atlantic and Pacific multidecadal oscillations and Northern Hemisphere temperatures. *Science* **347**, 988–991 (2015).
44. Chen, S., Wu, R. & Chen, W. The changing relationship between interannual variations of the North Atlantic Oscillation and Northern Tropical Atlantic SST <https://doi.org/10.1175/JCLI-D-14-00422.1> (2015).
45. Walter, K. & H.-F. Graf. On the changing nature of the regional connection between the North Atlantic Oscillation and sea surface temperature. *J. Geophys. Res.* **107**(D17), 4338, ACL 7-1–ACL 7-13(2002).
46. Huang, B., Schopf, P. S. & Shukla, J. Intrinsic Ocean–Atmosphere Variability of the Tropical Atlantic Ocean. *J. Clim.* **17**, 2058–2077 (2004).
47. Huang, B. & Shukla, J. Ocean–Atmosphere Interactions in the Tropical and Subtropical Atlantic Ocean. *J. Clim.* **18**, 1652–1672 (2005).
48. Dunstone, N. et al. Skilful predictions of the winter North Atlantic Oscillation one year ahead. *Nat. Geosci.* **9**, 809–814 (2016).
49. Zhu, Z., Feng, Y., Jiang, W., Lu, R. & Yang, Y. The compound impacts of sea surface temperature modes in the Indian and North Atlantic oceans on the extreme precipitation days in the Yangtze River Basin. *Clim. Dyn.* **61**, 3327–3341 (2023).
50. Ayarzagüena, B., Ineson, S., Dunstone, N. J., Baldwin, M. P. & Scaife, A. A. Intraseasonal effects of El Niño–Southern Oscillation on North Atlantic Climate. <https://doi.org/10.1175/JCLI-D-18-0097.1> (2018).
51. Jiménez-Esteve, B. & Domeisen, D. I. V. The tropospheric pathway of the ENSO–North Atlantic teleconnection. <https://doi.org/10.1175/JCLI-D-17-0716.1> (2018).
52. Mezzina, B., García-Serrano, J., Bladé, I. & Kucharski, F. Dynamics of the ENSO teleconnection and NAO variability in the North Atlantic–European Late Winter. <https://doi.org/10.1175/JCLI-D-19-0192.1> (2020).
53. Scaife, A. A. et al. Tropical rainfall, Rossby waves and regional winter climate predictions. *Q. J. R. Meteorol. Soc.* **143**, 1–11 (2017).
54. Scaife, A. A. et al. ENSO affects the North Atlantic Oscillation 1 year later. *Science* **386**, 82–86 (2024).
55. Latif, M., Martin, T. & Bielke, I. Regional variation in extratropical North Atlantic air–sea interaction 1960–2020. *Geophys. Res. Lett.* **51**, e2024GL108174 (2024).
56. Huang, B. et al. Extended reconstructed sea surface temperature, version 5 (ERSSTv5): upgrades, validations, and intercomparisons. <https://doi.org/10.1175/JCLI-D-16-0836.1> (2017).
57. Kalnay, E., & Coauthors. The NCEP/NCAR 40-Year Reanalysis Project. *Bull. Amer. Meteor. Soc.*, **77**, 437–472(1996).
58. Yu, L. & Weller, R. A. Objectively analyzed air–sea heat fluxes for the global ice-free oceans (1981–2005) <https://doi.org/10.1175/BAMS-88-4-527> (2007).
59. Yang, Y., Zhu, Z., Shen, X., Jiang, L. & Li, T. The Influences of Atlantic Sea Surface Temperature Anomalies on the ENSO-Independent Interannual Variability of East Asian Summer Monsoon Rainfall. *J. Clim.* **36**, 677–692 (2023).
60. Lau, N. & Holopainen, E. O. Transient Eddy Forcing of the Time-Mean Flow as Identified by Geopotential Tendencies. *J. Atmos. Sci.* **41**, 313–328 (1984).
61. Ren, H.-L., Jin, F.-F., Kug, J.-S. & Gao, L. Transformed eddy-PV flux and positive synoptic eddy feedback onto low-frequency flow. *Clim. Dyn.* **36**, 2357–2370 (2011).
62. Vallis, G. K. *Atmospheric and Oceanic Fluid Dynamics. Atmospheric and Oceanic Fluid Dynamics.* <https://doi.org/10.2277/0521849691> (2006).
63. Hendon, H. H. & Hartmann, D. L. Variability in a Nonlinear Model of the Atmosphere with Zonally Symmetric Forcing. *J. Atmos. Sci.* **42**, 2783–2797 (1985).
64. Hoskins, B. J., James, I. N. & White, G. H. White. The shape, propagation and mean-flow interaction of large-scale weather systems. *J. Atmos. Sci.* **40**, 1595–1612 (1983).
65. Lau, N. Variability of the observed midlatitude storm tracks in relation to low-frequency changes in the circulation pattern. *J. Atmos. Sci.* **45**, 2718–2743 (1988).
66. Trenberth, K. E. An assessment of the impact of transient eddies on the zonal flow during a blocking episode using localized Eliassen–Palm flux diagnostics. *J. Atmos. Sci.* **43**, 2070–2087 (1986).

## Acknowledgements

This work was jointly supported by the National Natural Science Foundation of China (42122034, 42075043, U2442207), the Youth Innovation Promotion Association (2021427) and West Light Foundation (xbzg-zdsys-202215) of the Chinese Academy of Sciences, Key Talent Projects in Gansu Province, Central Guidance Fund for Local Science and Technology Development Projects in Gansu Province (No.24ZYQA031).

## Author contributions

H.Y. proposed and conceived the study. S.C. plotted the figures. S.C. and H.Y. conducted paper writing and conducted the analyses. J.H. and Z.H. provided additional thoughts and helped revise the manuscript. H.W. participated in the geopotential height tendency anomalies analysis. X.W. revised the manuscript. S.C. prepared the manuscript with contributions from all the authors.

## Competing interests

The authors declare no competing interests.

## Additional information

**Supplementary information** The online version contains supplementary material available at <https://doi.org/10.1038/s41612-024-00882-0>.

**Correspondence** and requests for materials should be addressed to Haipeng Yu.

**Reprints and permissions information** is available at <http://www.nature.com/reprints>

**Publisher's note** Springer Nature remains neutral with regard to jurisdictional claims in published maps and institutional affiliations.

**Open Access** This article is licensed under a Creative Commons Attribution-NonCommercial-NoDerivatives 4.0 International License, which permits any non-commercial use, sharing, distribution and reproduction in any medium or format, as long as you give appropriate credit to the original author(s) and the source, provide a link to the Creative Commons licence, and indicate if you modified the licensed material. You do not have permission under this licence to share adapted material derived from this article or parts of it. The images or other third party material in this article are included in the article's Creative Commons licence, unless indicated otherwise in a credit line to the material. If material is not included in the article's Creative Commons licence and your intended use is not permitted by statutory regulation or exceeds the permitted use, you will need to obtain permission directly from the copyright holder. To view a copy of this licence, visit <http://creativecommons.org/licenses/by-nc-nd/4.0/>.

© The Author(s) 2024